*Huadong Yang, et. al. International Journal of Engineering Research and Applications*
*www.ijera.com*
*ISSN: 2248-9622, Vol. 12, Issue 5, (Series-I) May 2022, pp. 01-06*

RESEARCH ARTICLE OPEN ACCESS

# Experimental study on the effect of laser power on the forming quality of selective laser melting

Huadong Yang**, Shuai Tao
*(Department of Mechanical Engineering, North China Electric Power University, Baoding, China, 071000)*

**ABSTRACT**
In this paper, Inconel 718 of nickel-based superalloytest pieces were prepared by selectivelaser melting technology. The test pieces of Inconel 718 material printed under different process parameters were processed and their internal defects were observed. The influence of laser power and volume energy density on the forming quality of the test pieces during selective laser melting was studied. The results show that the bulk energy density is positively correlated with the forming quality of the test piece, and the laser power is too small to easily form holes and unfused defects.

***Keywords-*** Selective LaserMelting, Process Parameters, Bulk Energy Density, Forming Quality

---

Date of Submission: 25-04-2022 Date of Acceptance: 07-05-2022

---

## I. INTRODUCTION

As an advanced manufacturing technology that integrates machining technology, laser technology and material science, additive manufacturing technology emerged in the 1980s and developed rapidly. This technology uses lasers or ion beams to melt metal materials, non-metallic materials and biological materials, and directly manufactures the parts layer-by-layer from the digital model of the parts to perform near-net-shape parts [1]. Compared with subtractive manufacturing, this technology has more advantages, such as high degree of design freedom and high material utilization rate [2,3]. Additive manufacturing technology, especially for metal materials has been focused on by many researchers due to above advantages.

For metal parts with smaller size, selectivelaser melting (SLM) technology is one of the important technologies of near-net shape, and it is also an important part of additive manufacturing technology. It is widely used in aerospace, medicine and other fields [4,5]. Compared with other additive manufacturing technologies, SLM technology is faster, more efficient, and more promising [6]. For SLM, software is used to discretize the established 3D model to obtain laser scanning information. Before scanning, the processing chamber is filled with inert gas. During processing, the laser beam is moved to scan the paved metal powder based on the obtained laser scan information. After one layer is processed, the substrate is lowered by one layer thickness, and powder spreading and scanning are repeated to form the desired parts [7].

In recent years, there have been many studies on SLM. Researchers have used experimental, finite element, discrete element and other methods to study the influence of material properties, process parameters, scanning methods and other factors on the molding quality. Guo M et al. [8]studied the effect of the particle size of tungsten powder on the laser absorptivity during the laser selective melting process, and found that a larger particle size would lead to a decrease in the laser absorptivity. Niu W et al.[9] used SLM technology to prepare Inconel 718 alloy, and studied the effect of laser selective melting process on Inconel 718 alloy. PromoppatumP et al.[10] developed a finite element framework to predict the development of residual stress in parts in laser cladding with Inconel 718. Ahmed H[11] used the ANSYS APDL module to carry out the finite element simulation of the SLM forming process for 316L stainless steel powder, and analyzed the relationship between its temperature field, stress field, and the size of the molten pool and the scanning speed. LiuB et al. [12] developed a new model to conduct SLM single-pass simulation of Ti-6Al-4V powder and compared with experiments to study the defect threshold and keyhole transition of molten pool geometry and insufficient fusion.The correlation between weld pool geometry and underfusion defect threshold and keyhole transition is investigated, and the method by which the model can rapidly predict weld pool cross-sectional geometry is analyzed. Zhang X et al. [13] simulated the process of selective laser melting of 316L stainless steel by finite element, and explored the influence of process parameters such as laser power, scanning speed and scanning distance

on the forming quality. GU H et al. [14]used the discrete element method to establish a multi-track, multi-layer, multi-material laser selective melting model, and simulated the powder deposition process of various materials under different deposition modes. Baicheng Z et al.[15] used pre-optimized process parameters to electrochemically polish the surface of SLM Inconel 718 pipe fittings (Electrochemical polishing, ECP). Three-dimensional surface profiler and scanning electron microscopy (SEM) were used to characterize the surface morphology and roughness changes of Inconel 718 pipe fittings. At the same time, in order to determine the mechanical properties of the surface, nanoindentation tests were carried out on the original sample surface and the sample surface after ECP. JPKruth[16] studied the influence of 6 different scanning methods on the deformation of SLM formed parts. The study found that different scanning methods will cause different temperature gradient changes, resulting in different thermal stress and different deformation. Sankhya M [17] and others also simulated the SLM forming process, studied the influence of different scanning methods on the temperature field, and found that the Z-type scanning method is most conducive to achieving a uniform temperature field.

For the research on the forming quality in different process parameters, numerical simulation is usually adopted at present, so the construction of the coupling relationship between the process parameters and the internal defects is lacking. In this paper, by preparing Inconel718 specimens under different process parameters and using low-cost experimental research methods, the relationship between laser power and internal defects of SLM parts is explored.

## II. EXPERIMENTAL PROCESS

### 1. Experimental materials and instruments

During this experiment, the test pieces was printed by the Beijing E-Plus-3D EPM350 printer. The maximum power of a single laser is 200W, the maximum molding size is 305mm×305mm×450mm, the layer thickness is 0.02~0.12mm, and the maximum scanning speed is 8000mm/s. The printer is protected by argon gas, and the oxygen content of the chamber is not more than 100ppm. And the printing material is nickel-based superalloy 718 powder produced by Beijing E-Plus-3D Co., Ltd. The monitoring system adopts the AM & IM-PMS model made by Xi'an Aerospace Electromechanical Intelligent Manufacturing Co., Ltd.

### 2. Experimental process parameters

The purpose of this paper is to study the influence of laser power on the forming quality. Therefore, the Z-scanning method, which is common and has the best forming quality, is selected for all samples during the printing process, and the thickness of the powder layer is set to 0.04mm. Combined with the bulk energy density formula, the relationship between defect formation and process parameters was studied.

In the experiment, different laser power, scanning speed and scanning spacing were selected, and 12 cube test pieces with the size of 5mm×5mm×5mm were printed. There are two different laser powers, 210W and 270W, two different scanning speeds, 800 mm/s and 1000 mm/s, and three different scanning distances, 0.07 mm, 0.1 mm, and 0.13 mm. The energy density formula is shown in formula (1) [18]:

$$w = \frac{P}{vsh} \quad (1)$$

In the formula, w is the volume energy density ( J·mm$^{-3}$), P is the laser power (W), v is the laser scanning speed (mm/s), s is the scanning distance (mm), h is the powder thickness (mm). Specimen parameters are shown in Table 1-1. It can be seen from formula (1) that the volume energy density is proportional to the laser power and inversely proportional to the laser scanning speed, scanning distance and powder thickness.

**Table 1 Printing process parameters of different test pieces**

| Test-piece number | Laser Power $/W$ | Scanning Speed $/(mm \cdot s^{-1})$ | Scanning Distance $/(mm)$ | Energy Density $/(J \cdot mm^{-3})$ |
|---|---|---|---|---|
| 1 | 210 | 800 | 0.07 | 93.75 |
| 2 | 210 | 800 | 0.1 | 65.63 |
| 3 | 210 | 800 | 0.13 | 50.48 |
| 4 | 210 | 1000 | 0.07 | 75.00 |
| 5 | 210 | 1000 | 0.1 | 52.50 |
| 6 | 210 | 1000 | 0.13 | 40.38 |
| 7 | 270 | 800 | 0.07 | 120.54 |
| 8 | 270 | 800 | 0.1 | 84.38 |
| 9 | 270 | 800 | 0.13 | 64.90 |
| 10 | 270 | 1000 | 0.07 | 96.43 |
| 11 | 270 | 1000 | 0.1 | 67.50 |
| 12 | 270 | 1000 | 0.13 | 51.92 |

In order to obtain the internal molding defect map, sandpaper was used to grind the thickness and scratches of the printed specimen, and electron microscope scanning was used at different depths to obtain five sets of images, and the sampling depth difference between the adjacent two sets of images was 1 mm. Before scanning, rinse the ground and polished specimen with clean water, drop an appropriate amount of anhydrous ethanol on the surface of the specimen, and then air-dry it, so as to avoid water stains on the specimen affecting the observation results during observation. After

air-drying, place them under an electron microscope to observe and capture screenshots of internal defects. Since the electron microscope still cannot observe the entire surface of the specimen at the lowest magnification, it is necessary to adjust the electron microscope tray to move the observation position of the specimen, and capture the complete specimen image in multiple areas. After selection, the most representative pictures in each group were selected for this experiment.

## III. EXPERIMENTAL RESULT ANALYSIS

To analyze the influence of different laser powers on the forming quality, first of all, it is necessary to ensure that the two parameters of scanning speed and scanning distance are the same. According to the process parameters of preparing the test pieces, samples with the same scanning speed and scanning distance under different laser powers are selected. In the experiment, two different laser powers (210W and 270W), two different scanning speeds ( 800mm/s and 1000 mm/s) and three different scanning distances (0.07 mm, 0.1 mm, and 0.13 mm) were chosen. The parameters of scanning speed and scanning distance are now set to a constant. Invariably, there are theoretically 6 sets of combinations (2 types of scanning speed × 3 types of scanning pitch). The actual optional combinations are shown in Table 2. Two adjacent groups from top to bottom are divided into six groups in total, 1 and 7, 2 and 8, 3 and 9, 4 and 10, 5 and 11 , 6 and 12.

**Table 2 Data grouping under different laser powers**

| Test-piece Number | Laser Power/W | Scanning Speed/(mm/s) | Scanning Pitch/mm |
|---|---|---|---|
| 1 | 210 | 800 | 0.07 |
| 7 | 270 | 800 | 0.07 |
| 2 | 210 | 800 | 0.1 |
| 8 | 270 | 800 | 0.1 |
| 3 | 210 | 800 | 0.13 |
| 9 | 270 | 800 | 0.13 |
| 4 | 210 | 1000 | 0.07 |
| 10 | 270 | 1000 | 0.07 |
| 5 | 210 | 1000 | 0.1 |
| 11 | 270 | 1000 | 0.1 |
| 6 | 210 | 1000 | 0.13 |
| 12 | 270 | 1000 | 0.13 |

For test piece 1 and7, the scanning speed is 800mm/s and the scanning distance is the same as 0.07mm, and the power is 210W and 270W respectively. The five groups of internal defects observed in the test piece 1 and 7 under the electron microscope are shown in Figure 1. It can be clearly seen from group a, group c and group e that the test piece 1 has more defects than test piece 7, and the defect types are mainly pores, and there are also some unfused phenomena (test piece 1, group d).

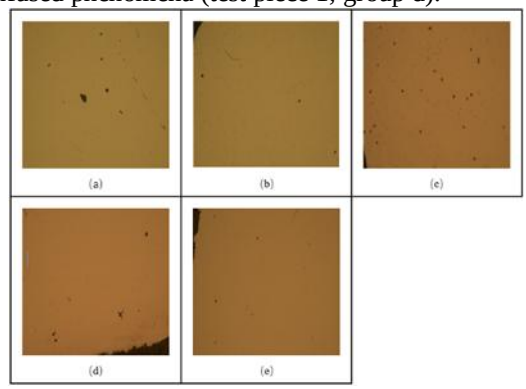


(I)Test piece 1

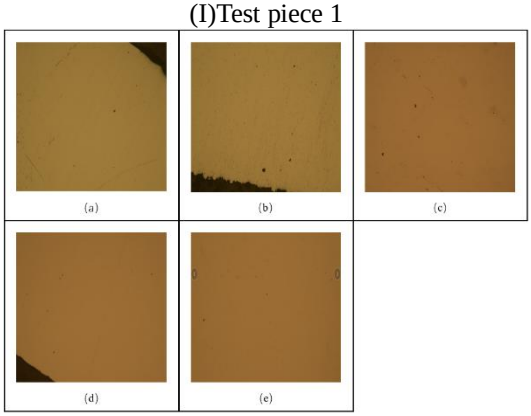


(II)Test piece7

**Figure 1 Comparison diagram of test piece 1 and 7**

For test piece 2 and 8, the scanning speed is 800mm/s and the scanning interval is the same as 0.1mm, and the power is 210W and 270W respectively. The five groups of internal defects observed in the test piece 2 and 8 under the electron microscope are shown in Figure 2. Except for group d, other groups can clearly see that the internal defects of test piece 2 are more than those of test piece 8. The defect types are mainly pores, and there are also a small amount of cracks (compared to test piece 2,group b). ) and lack of fusion (groups a and d of test piece 8, and group e of test piece2).

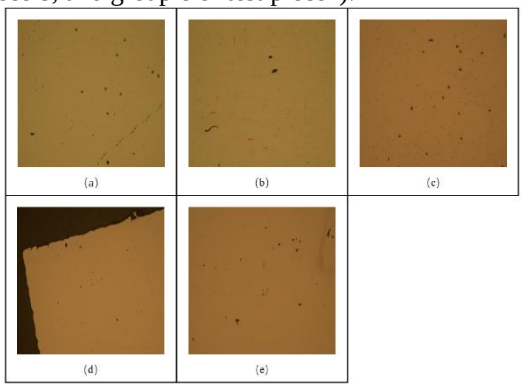


(I)Test piece2

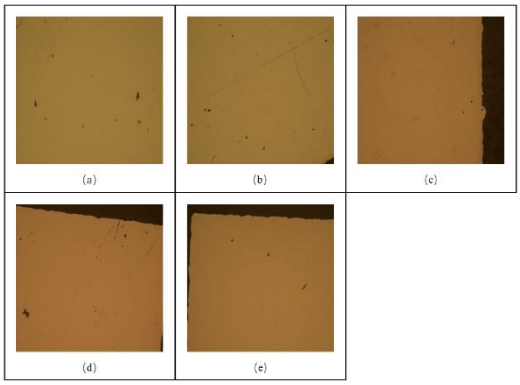


(II)Test piece 8

**Figure 2 Comparison diagram of test piece 2 and 8**

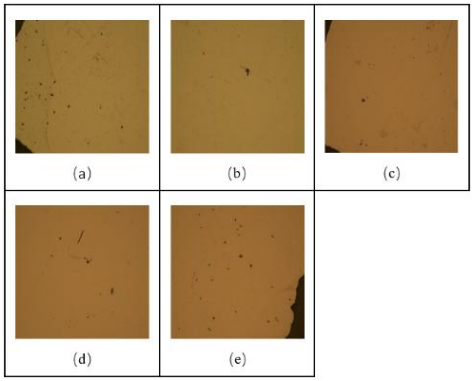


(I)Test piece 3

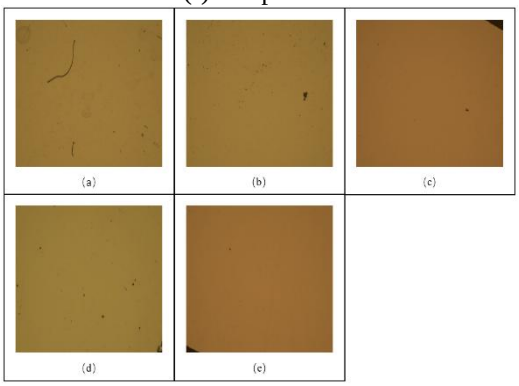


(II)Test piece 9

**Figure 3 Comparison diagram of test piece 3 and 9**

For test piece 3 and 9, the scanning speed is the same as 800mm/s and the scanning interval is 0.13mm/s, and the power is 210W and 270W, respectively. The five groups of internal defects of test piece 3 and 9 observed under the electron microscope are as follows: shown in Figure 3. Except for groups b and c, it can be clearly seen that the number of internal defects in test piece 3 is more than that of test piece 9, and the defect types are mainly pores, and some are lack of fusion (in group b of the two test pieces). There is lack of fusion phenomenon and cracks (in the comparison, there is a relatively obvious crack in the test piece 9 group a, and there is a shorter crack in the test piece 3).

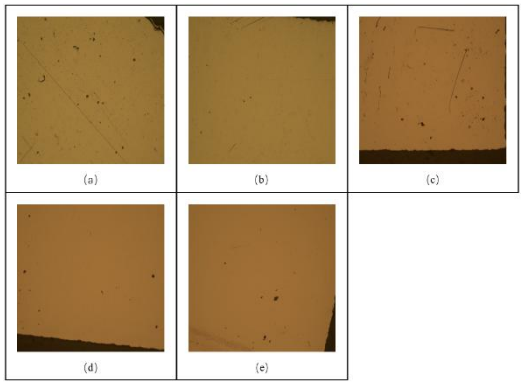


(I)Test piece 4

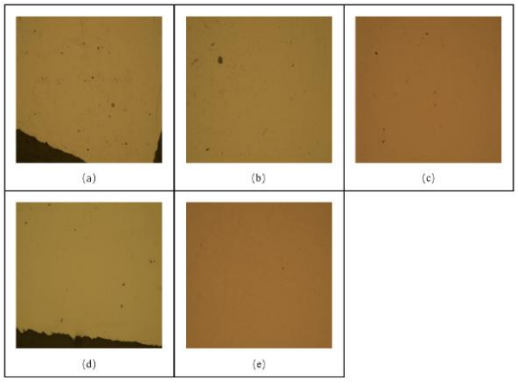


(II)Test piece 10

**Figure 4 Comparison diagram of test piece 4 and 10**

For test piece 4 and 10, the scanning speed of 1000 mm/s and the scanning distance of 0.07 mm are the same, and the powers are 210 W and 270 W respectively. The five groups of internal defects of test piece 4 and 10 observed under the electron microscope are shown in the figure 4. From the groups a, c and e, it can be clearly seen that the internal defects of the test piece 4 are more than those of the test piece 10. The types of defects are mainly pores, and there is also a small amount of unfused phenomenon. Comparing the images of group a of the two test pieces, it can be found that obvious scratches are existed in the test piece 4.

For test piece 5 and 11, the scanning speed is 1000mm/s and the scanning distance is the same as 0.1mm, and the power is 210W and 270W respectively. The five groups of internal defects of test piece 5 and 11 observed under the electron microscope are shown in Figure 5. Except for groups b and d, the other three groups can clearly see that the internal defects of the test piece 5 are more than those of the test piece 11, and the defect types are mainly pores. Among them, a long crack is existed in group d of test piece 11.

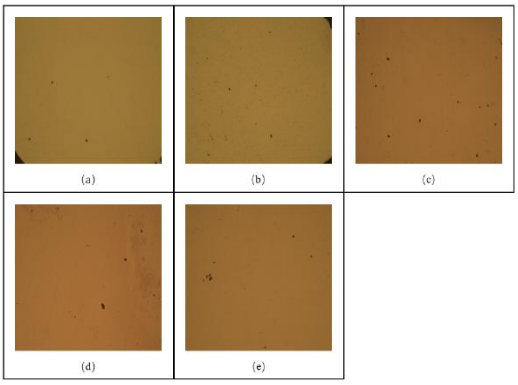


(I)Test piece 5

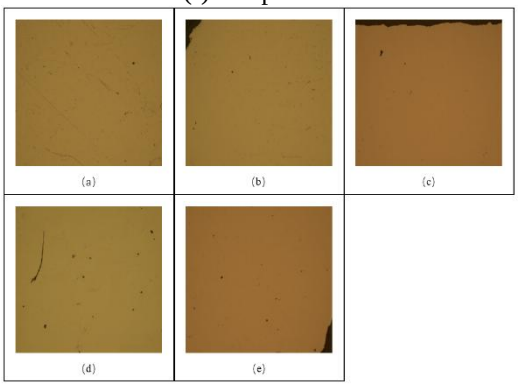


(II)Test piece 11

**Figure5 Comparison diagram of test piece 5 and 11**

For test piece 6 and 12, the scanning speed is the same as 1000mm/s and the scanning distance is 0.13mm, and the power is 210W and 270W, respectively. The five groups of internal defects of test piece 6 and 12 observed under the electron microscope are shown in Figure6. Among them, due to the excessive internal defects of the test piece 6, multiple results are required to reflect the defect distribution. It can be clearly seen from all the groups that the internal defects of the test piece 6 are more than those of the test piece 12, and the defect types are mainly lack of fusion, and there are also some pores and cracks (group a of the test piece 6, group c of the test piece 12).

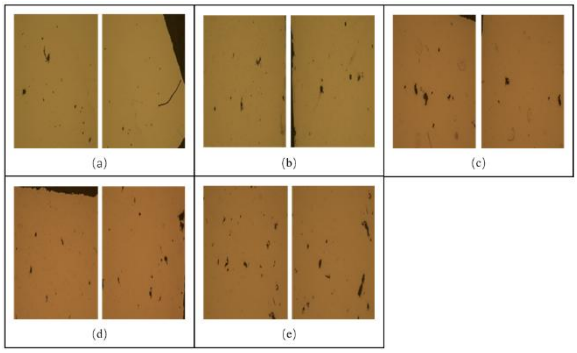


(I)Test piece 6

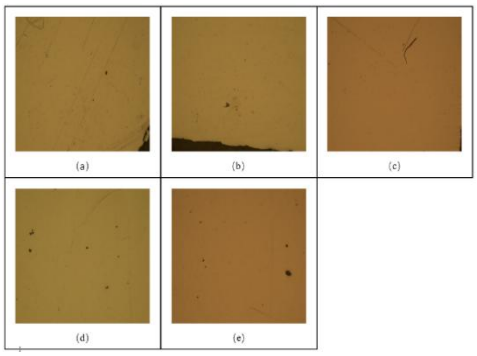


(II)Test piece 12

**Figure 6 Comparison diagram of test piece 6 and 12**

From these six sets of control experiments, it can be intuitively concluded that the specimens with higher laser power have smaller probability of forming internal defects (the smaller the number, size and type is ). Further analysis according to the picture shows that with the increase of laser power, the number of pore defects in the sample decreases significantly, and the size of the pores also decreases relatively. Under the condition that the scanning speed and scanning distance remain unchanged, the laser power is increased from 210W to 270W, and the original large number and large pore defects in the surface structure of the sample have basically disappeared.

When the laser power increases, the length, width and depth of the molten pool will also increase, the powder in the area will be completely melted, the maximum temperature in the molten pool and the flow rate of the liquid metal will increase, and it will be easier to form good molding quality.When the laser power decreases, the energy absorbed by the powder layer is reduced, and the length, width and depth of the molten pool are also reduced, and the powder is easily melted incompletely. Therefore, if the laser power is too small, holes will appear inside the test piece.

## IV. CONCLUSION

(1) In the process of selective laser melting, if the laser power is 210W to 270W, the scanning speed is 800mm/s to 1000 mm/s, and the scanning distance is within the parameter range of 0.07 mm to 0.13 mm, when the laser power is reduced, defects are easily caused.

(2) According to the volume energy density formula, the volume energy density is proportional to the laser power, and inversely proportional to the scanning speed and scanning distance, so the volume energy density is $40.38J{\cdot}mm^{-3}$ to $120.54J{\cdot}mm^{-3}$, the body energy density is positively correlated with the molding quality. If the bulk energy density is too low, the discrete powder in the region cannot absorb enough energy, resulting in insufficient powder

melting and the formation of defects such as holes.

(3) From the results of the three groups of test pieces with similar energy densities, the test piece 1 and 8, the test piece 4 and 11, and the test piece 2 and 9, it can be seen that within the process parameters set in the experiment, the small laser power has a significant effect on the formation of voids and unfused defects.

## REFERENCES

[1]. Huang Y N, Yang L, Li X L.Research progress and prospect of 3D printing metal structures. Proceedings of the 17th (ISSF-2021) Academic Exchange Conference and Teaching Seminar of China Steel Structure Association Structural Stability and Fatigue Branch. Beijing,China, 2021 : 170-174.

[2]. Wu G, Hu Y, Zhu W, et al. Research Status and Development Trend of Laser Additive Manufacturing Technology. 2017 4th International Conference on Information Science and Control Engineering (ICISCE).Changsha, PEOPLES R CHINA, IEEE Computer Society, 2017 : 1210-1213.

[3]. Liang Z L, Sun Z G, Zhang S C, Chang H.Application and research status of numerical simulation in laser selective melting. Journal of Aerospace Manufacturing Technology,2018,61(22):87-91+97.

[4]. Wang Z M, Huang W P, Zeng X Y.Development status and trend of laser selective melting forming equipment.Precision Forming Engineering, 2019, 11(04):21-28.

[5]. Liu C, Ma X C, Ma H B.Influence of process parameters on the density of 316L stainless steel formed by SLM and the manifestation of defects.Journal of Thermal Processing,2021,50(12):44-49.

[6]. Wu G,Hu Y,Zhu W,et al. Research Status and Development Trend of Laser Additive Manufacturing Technology.20174th International Conference on Information Science and Control Engineering (ICISCE).Changsha,PEOPLES R CHINA,IEEE Computer Society,2017:1210-1213.

[7]. Hu M J, Ji L K, Ma Q R, Chi Q.Research on Laser Additive Manufacturing Technology and Current Situation. Petroleum Pipes and Instruments,2019,5(05):1-6.

[8]. [8]GuoM,GuD,Xi L, et al. Formation of scanning tracks during Selective Laser Melting (SLM) of puretungsten powder: Morphology, geometric features and forming mechanisms. International Journal of Refractory Metals and Hard Materials, 2019, 79: 37-46.

[9]. Niu W. Effect of Heat Treatment on Microstructure and Properties of Inconel 718 Alloy Formed by Laser Selective Melting. Beijing,Beijing Industry University, 2016.

[10]. Promoppatum P,Uthaisangsuk V. Part scale estimation of residual stress development in laser powder bed fusion additive manufacturing of Inconel 718. Finite Elements in Analysis and Design,2021,189(7):1-15.

[11]. Hussein A, HaoL,Yan C,et al. Finite element simulation of the temperature and stress fields in single layers built without-support in selective laser melting. Materials & Design,2013,52(1):638-647.

[12]. Liu B,Fang G,Lei L. An analytical model for rapid predicting molten pool geometry of selective laser melting (SLM). Applied Mathematical Modelling, 2021,92(4):505-524.

[13]. Zhang X,Chen L,Zhou J, et al. Simulation and Experimental Studies on Process Parameters, Microstructure and Mechanical Properties of Selective Laser Melting of Stainless Steel 316L. Journal of the Brazilian Society of Mechanical Sciences and Engineering, 2020, 42(8): 1-14.

[14]. GuH,WeiC,Li L, et al. Multi-physics modelling of molten pool development and track formation in multi-track, multi-layer and multi-material selective laser melting. International Journal of Heat and Mass Transfer, 2020, 151: 119458.

[15]. Baicheng Z,Xiaohua L,JiamingB,et al. Study of selective laser melting (SLM) Inconel 718 part surface improvement by electrochemical polishing. Materials & Design. 2017,116:531-537.

[16]. Kruth J P,Froyen L,Van Vaerenbergh J,et al. Selective laser melting of iron-based powder. Journal of Materials Processing Technology,2004,149(1-3):616-622.

[17]. Klotzbach U,Mohanty S,Tutum C C,et al. Cellular scanning strategy for selective laser melting:evolution of optimal grid-based scanning path and parametric approach to thermal homogeneity. Conference on Laser-Based Micro- and Nanopackaging and Assembly VII (LBMP) as a part of LASE Photonics West. San Francisco, CA,SPIE-INT SOC OPTICAL ENGINEERING.2017.

[18]. LV J J, Jia C Z, Yang J C.Effect of Laser Energy Density on the Quality of Laser Selective Melting. Journal of Thermal Process, 47(20):156-159.